Investigation into MQCA based low power Digital logic Design Methodology

Khan Shahnawaz Inteshar

A Dissertation Submitted to

Indian Institute of Technology Hyderabad

In Partial Fulfillment of the Requirements for
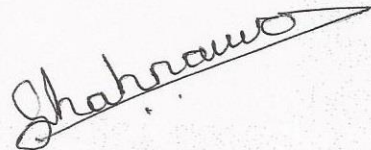
The Degree of Master of Technology

भारतीय प्रौद्योगिकी संस्थान हैदराबाद
Indian Institute of Technology Hyderabad

Department of Electrical Engineering

June, 2015

Declaration

I declare that this written submission represents my ideas in my own words, and where others' ideas or words have been included, I have adequately cited and referenced the original sources. I also declare that I have adhered to all principles of academic honesty and integrity and have not misrepresented or fabricated or falsified any idea/data/fact/source in my submission. I understand that any violation of the above will be a cause for disciplinary action by the Institute and can also evoke penal action from the sources that have thus not been properly cited, or from whom proper permission has not been taken when needed.

Khan Shahnawaz Inteshar

EE13M1013

Approval Sheet

This thesis entitled "Investigation into MQCA Based Low Power Digital Logic Design Methodology" by Khan Shahnawaz Inteshar is approved for the degree of Master of Technology from IIT Hyderabad.

External Examiner

Internal Examiner

Adviser

Co-Adviser

Chairman

Acknowledgements

Dedicated to

My Parents and My Gurus

Abstract

The use of the phenomenon of magnetism for information processing goes back to the end of XIX century. In 1888, Oberlin Smith suggested the use of permanent magnetic impressions for the recording of sound. The recording of the human voice on a steel piano wire was first carried out in 1898 by a Danish inventor Valdemar Poulsen, whose invention gave rise some 30 years later to a magnetic tape recording industry. With the creation of the first computers, the use of magnetic storage elements such as tapes, cores, and later magnetic disks, have become widespread. Early on in the computer era, several attempts were made to develop all-magnetic logic, most notably using such devices as laddics and transuxors. These devices were magnetic ferrite elements of complex shape, interconnected by windings of copper wire. For example, the laddic was an element that had the appearance of a small ladder cut out of a ferrite with wire windings serving as inputs and outputs. By controlling the switching path through the structure, any Boolean function could be produced. The switching speeds of a few tenths of a microsecond and repetition rates of a few hundred kHz were reported. During the infancy of semiconductor processing, these numbers looked rather attractive. Moreover, even almost half a century later, all-magnetic logic devices are still unsurpassed in terms of their reliability, nonvolatile data retention and radiation hardness.

Contents

Chapter 1

Introduction

Cellular Automata involving field interaction for logic computation has been the alternative computing paradigm that offers interconnect-free design architecture, and hence, provides the scope for realizing low power circuits in the nanometer scale regime. The Quantum-dot-cellular automata (QCA), a category of Cellular Automata, uses Columbic interaction among electrons to realize logic functionality [1], [2], [3], [4]. However, QCA's have been fabricated and functionally verified only in the cryogenic temperatures. Many interesting observations related to energy dissipation in QCA can be found in [5], [6], [7]. For example, energy dissipation increased when the tunneling energy through the clock was enhanced. Also, energy dissipation was not reduced with scaling. In fact when the cell size was 10 nm, average energy dissipation was 12μeV whereas energy dissipation for a 40 nm cell was calculated to be 1.8μeV. In spite of such low energy dissipation in the computing systems, ITRS roadmap [8], reported reduced interest in Electronic-QCA due to power requirements to achieve ultra-low temperature circuit operation.
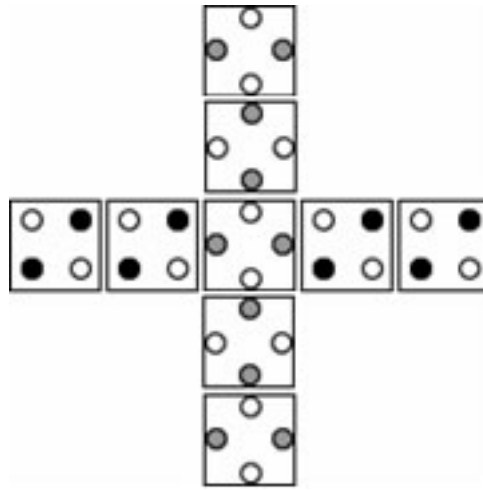
Figure 1-1: Representation of Quantum-Dot Cellular Automata

Quantum-dot cellular automata (QCA) is deemed a potential candidate to replace or supplement CMOS electronic circuits at the end of the roadmap. QCA effects computation through the interaction of fields, and requires the transfer of charge only within a small, confined volume, called a QCA cell. In most cases the fields are electrical in nature, and electrons move within a cell in response to the charge positions of neighboring cells. It has been shown in Figure 1-1 theoretically that an array of cells can be used to effect complex computations, similar to that of a CMOS processor.

Molecular Cellular Automata and Atomic Cellular Automata are the other two offshoots of Cellular Automata involving field coupled computing. While both architectures have displayed good promise for room temperature operations, research is still under progress to develop a stable structure of the molecules [9], [10], [11], [12]. The neighbor interaction among similar cells is also a subject of study.
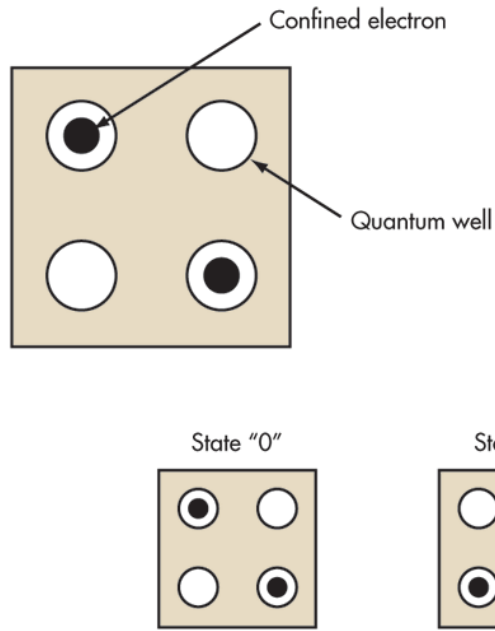
Figure 1-2: Schematic of Quantum Cellular Dot

Magnetic Quantum Cellular Automata (MQCA), the last member of this family till date, has been the most extensively researched phenomenon that has the ability to operate at room temperature. They have been successfully employed to demonstrate various logic elements including basic logic gates and horizontal and vertical wires. The two energy minimum states by virtue of their shape anisotropy enables them to represent stable binary logic. Switching between the states takes place through an external phenomenon named Clocking. Interconnect-free low power logic has been successfully demonstrated using MQCA.

1.1 Motivation

As mentioned above the magnetic quantum-dot cellular automata concept is a version of the field coupled QCA architecture that was first proposed in [13]. The original idea was introduced for a quantum dot system, in which electrons tunnel between the quantum dots under the influence of repelling

3

Coulomb forces. The basic QCA geometries and their functions are shown in Figure 1-2. An elementary building block contains four quantum dots in a square arrangement, having one dot in each corner.

Chapter 2

Literature survey

The use of magnetism for information storage processing goes back to the end of the 19th century [14, 15]. At the beginning of the 21st century, as the semiconductor industry faces difficulties for further down-scaling, several applications of magnetism for future logic and memory devices are proposed and investigated, such as the Magnetic Random Access Memory (MRAM) [16], the racetrack memory [17], as well as the magnetic Quantum-Dot Cellular Automata (MQCA) [18] recently referred to as nanomagnet logic (NML). All-magnetic information processing [19, 20] based on nanomagnets may become an attractive alternative to the electronic representation and information processing by naturally providing non-volatility, radiation hardness, high integration density, and very low power dissipation [21]. Energy/performance gains over CMOS are possible as well [22].

NML is based on a new computational paradigm (QCA) invented at Notre Dame [23], and is built from single-domain nanomagnets (nanodots, dots). NML uses stray magnetic fields as a physical coupling mechanism between bistable building blocks, which are assembled into arrays, to perform binary logic functions. Basic NML structures, such as lines, gates,

and inverters have been experimentally demonstrated, and function at room temperature [24-26].

In the NML devices, the magnets are forced to be in a high-energy state by a magnetic field referred to as the clocking field. As the clocking field is removed, the magnets relax into one of their two stable, low energy states. Standalone magnets relax randomly into one of the two states. As the nanomagnets are placed several nanometers apart, the emanating field from the neighboring magnets defines their final states. The field of the driver magnet is referred to as the biasing field.

2.1 Purpose of MQCA
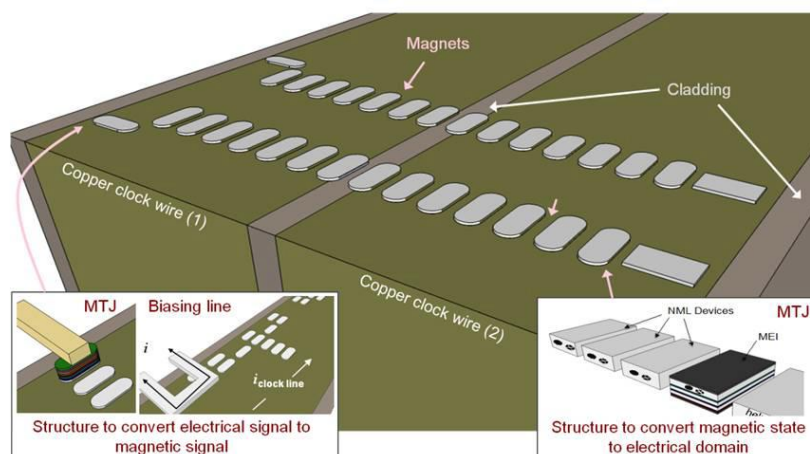
Figure 2-1: Schematic of envisioned structure for NML operation

The main goal is to fabricate a complete NML circuit, such as the one shown in Figure 2-1. The underlying copper wires are driven by a driver circuitry (not shown in the schematic). Current passing through these wires generates the clocking field for the NML structures, which are built on top of the wires. Although in this case, the required high current density needed to provide the sufficiently strong magnetic fields raises some issues [27]. The

clocking is set in such a way that the information propagates from left to right in the magnetic circuit. The envisioned biasing field for the nanomagnet circuit is provided locally either by a magnetic tunnel junction (MTJ) or by a biasing line, which converts an electrical signal to a magnetic signal [28]. At the output of the NML circuit, the MTJ converts the magnetic signal back to an electrical signal for possible further processing. This work focuses mostly on the engineering of the patterned nanomagnet layer.

Chapter 3

Nanomagnet logic gate design

The basic unit of NML is the nanomagnet. In previous works, identical nanomagnets were used to build NML structures with simple shapes, such as rectangles and ellipsoids. Some shape studies were performed on standalone magnets [29]. In addition to this advantage, shape engineering has other benefits as well. In the following sub chapters, we investigate the magnetic behavioral properties of nanomagnets with various aspect ratios (Section 3.1) and with different shapes (Section 3.2) to show possible programmability for NML gates. [30], and it has been shown that different shapes can have different sensitivity to fabrication variations.

3.1 Symmetrically shaped nanomagnets

A symmetrically shaped magnet has an energy barrier between two stable states, as shown in Figure 3-1, with the energy (E) vs. magnetization (H) landscape as shown. Consider a symmetric magnet that is subjected to a strong hard-axis field (indicated by the thick blue arrow pointing from left to right in Figure 3-1). For a large hard-axis external field, referred to as the "clocking field," the magnetization is pointing in the direction of the field, and favors neither the up or down direction, a condition referred to as
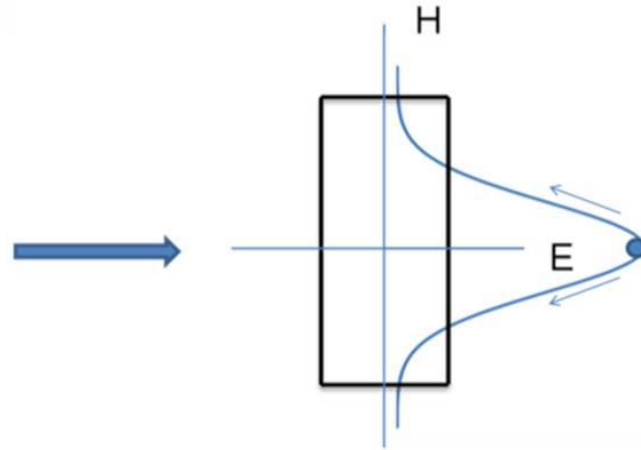
Figure 3-1: Energy landscape and clocking process of a symmetric, rectangular shape nanomagnet. The thick, blue arrow indicates the strong hard-axis clocking field. As the field is removed, the symmetric nanomagnet relaxes into one of the two energetically equivalent ground state.

"nulled." When the field is removed, the nanomagnet relaxes into one of the two energetically equivalent ground states, i.e., either pointing up or down. Even a small biasing field along the easy axis can influence which magnet ground state the magnetization will select. In Figure 3-1, the blue curve shows the potential landscape of the nanomagnet immediately after the removal of the nulling field. The presence of the energy barrier requires that an external field stronger than the nulling field is required to re-evaluate the magnet, i.e., set the magnet so that a new logic value, either up or down, can be written to it. It relaxes into a newly ordered state in accordance with any present biasing field. The magnet retains its new state without an externally applied field, since the size of the magnet is assumed to be larger than the superparamagnetic limit.

3.2 Symmetrically shaped nanomagnets

Shape engineering leads us to exploit the magnetic property of asymmetric nanomagnets. Most studies on single-domain magnets focused on symmetric

9

shapes with two, energetically equivalent ground states pointing along the easy axis (Figure 3-1). In this section, slanted-edge magnets are investigated.
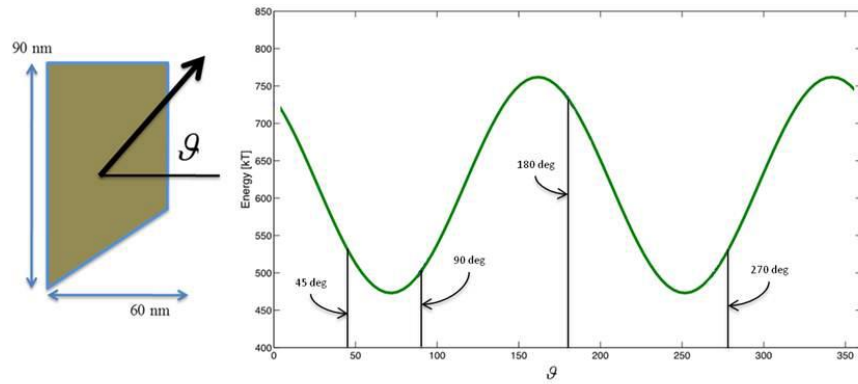

Figure 3-2: Simulation based on the single-domain model result for the slant nanomagnet energy landscape. The energy minima are shifted from the long geometrical axis, i.e., from the 90 deg and 270 deg magnetization directions.
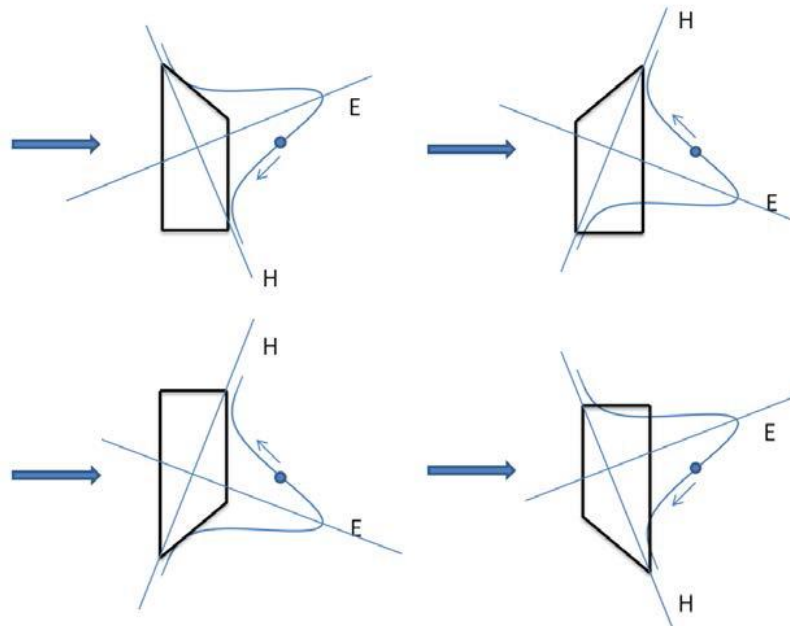

Figure 3-3: Energy curves of the slant magnets for different slant locations. The external magnetic field is applied from left to right shown by horizontal, thick, blue arrows. The thin line along the diagonal of the magnet corresponds to the effective easy axis.

A schematic of the asymmetric magnet having a slanted edge is shown in Figure 3-2 on the left side [31]. Simulations based on the single-domain model show that the asymmetry of the magnet shifts the entire

10

energy landscape of the magnet, whereby the energy minima are shifted as well by about 20 deg. The thin line along the diagonal of the magnet in Figure 3-2 corresponds to the effective easy axis. The energy maximum is perpendicular to this axis. The horizontally applied field is not precisely in the direction of the energy maximum, so the resulting energy of the magnet is to one side of the maximum, and falls toward the appropriate ground state when the field is removed. As a result of the tilted easy axis, the nanomagnet takes on a preferred magnetization direction, as summarized in Figure 3-3.

The schematic (Figure 3-3) lists all possible slant orientations and the corresponding overlaid energy diagrams, energy (E) vs. magnetization (H). The magnets in a) and d) relax into the downward pointing magnetization, and in b) and c) relax into the upward pointing direction. This specific shape can be exploited to reduce device footprint as shown below.
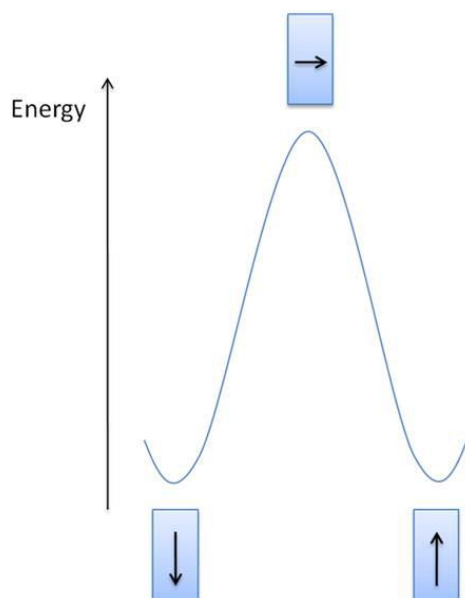
3.3   Nanomagnets in NML devices

Figure 3-4: Energy diagram of the magnets in different magnetization states. The magnet has low energy while magnetized along its long geometrical axis, and high energy when the magnetization is pointing along its short axis.

The nanomagnets inside the NML devices are aligned on a rectangular grid with their long axis oriented either horizontally or vertically. We apply an external field either along the horizontal or the vertical direction to set the magnetization state of each magnet; therefore, some magnets experience this field along their easy (long geometrical) axis and others along their hard (short geometrical) axis. The energies of these states are summarized in Figure 3-4. The easy axis magnetization flips the magnet into a stable and low energy state, and the hard axis magnetization provides an unstable, high-energy state. The energy difference between the two states extends from a few to few hundred electronvolts depending on the size and the shape of the magnet [32].
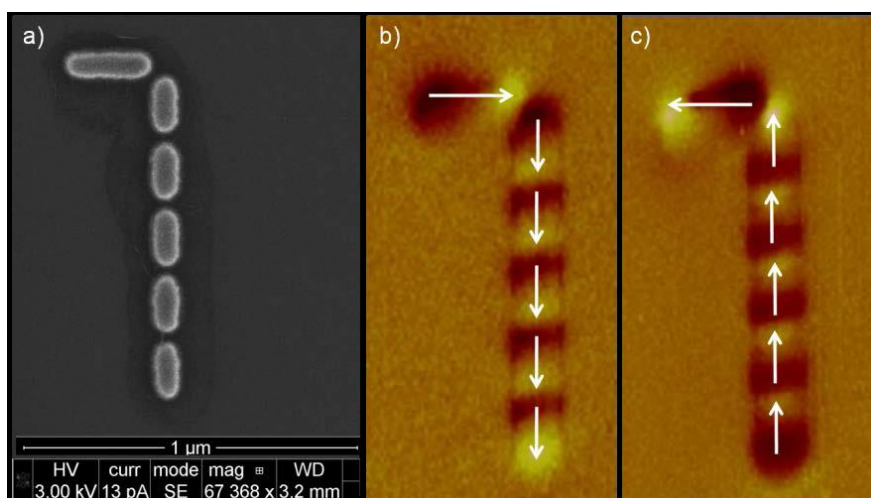
3.4   Nanomagnet Wire

Figure 3-5: a) SEM image of a 5-nanomagnet-long vertical wire with a horizontally aligned driver magnet. b) MFM image of the same wire for one magnetization state of the driver magnet and c) for the other. The information propagates from the driver magnet toward the bottom of the wire by ferromagnetic coupling.

The nanomagnet wire is the basic structure of the NML circuit library; therefore, the most often used building block of devices. Nanomagnets comprising NML wires can be coupled in one of two ways. One of these is the vertically aligned wire with ferromagnetically coupled (FC) magnets, and

the other is the horizontally aligned wire built from antiferromagnetically coupled (AFC) magnets. The orientation of the wire can be either horizontal (AFC) or vertical (FC). The FC wires can be as long as it is necessary to fulfill other design requirements, but in the AFC wire, every other magnet inverts the carried information, i.e., the wire length has to be an odd number to have the same bit value at the beginning and at the end of the wire.

The vertical wire is shown in the SEM image in Figure 3-5. The one horizontally aligned magnet on the top is the driver magnet; it initializes the entire wire through FC. Its dimensions are 60 nm X 240 nm. All magnets are 30 nm thick, and are separated by 25 nm. The wire is magnetized first by a horizontal pumping field pointing into the positive direction followed by a reverse field. MFM scan is performed after each magnetization to show the magnetization state of the vertical wire (Figure 3-5b and Figure 3-5c). The nanomagnets perform correctly and pass the information from the driver magnet through the wire according to the magnetization state of the driver magnet.
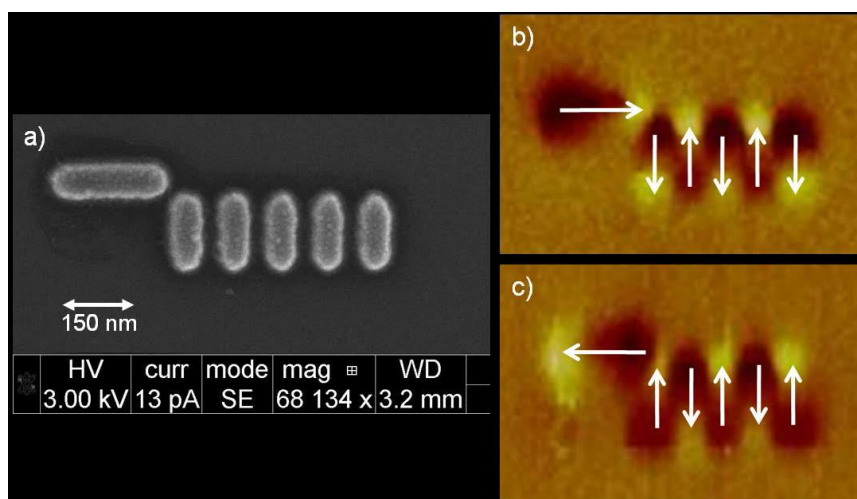

Figure 3-6: a) SEM image of a 5-nanomagnet-long horizontal wire with a horizontally aligned driver magnet. b) MFM image of the same wire for one magnetization state of the driver magnet and c) for the other. The information propagates from left to right, that is, from the region of strongest to weakest influence.

One horizontally aligned, five-magnet-long wire is shown in Figure 3-6a. Here, the information propagates from the horizontal driver magnet through the antiferromagnetically coupled magnets, i.e., from left to right. Two MFM images (Figure 3-6b and Figure 3-6c) show the magnetization of the same wire for two possible states of the driver magnet. The same external field is applied here as for the vertical wires.

Chapter 4

Nanomagnet Fabrication Techniques

The technology for fabricating arrays of nanomagnets is currently under development in the HDD and MRAM industrial research.

The patterned media development is still at an early stage. Fabrication techniques involve electron-beam lithography (EBL), X-ray and interference lithography, nanoimprinting, magnetic material deposition and pattern transfer. The deposition of the magnetic material is usually done by electroplating, sputtering or evaporation; the pattern transfer applies reactive ion etching (RIE) or low-energy ion irradiation. Focused ion beam (FIB) techniques are also under consideration [33,34].

There is a significant effort directed toward fabricating nanomagnets with an easy axis perpendicular instead of parallel to the surface, and many papers present fabrication of nanopillars [35], or patterning of metallic multilayers [36-38], which both provide out of plane domain orientation.

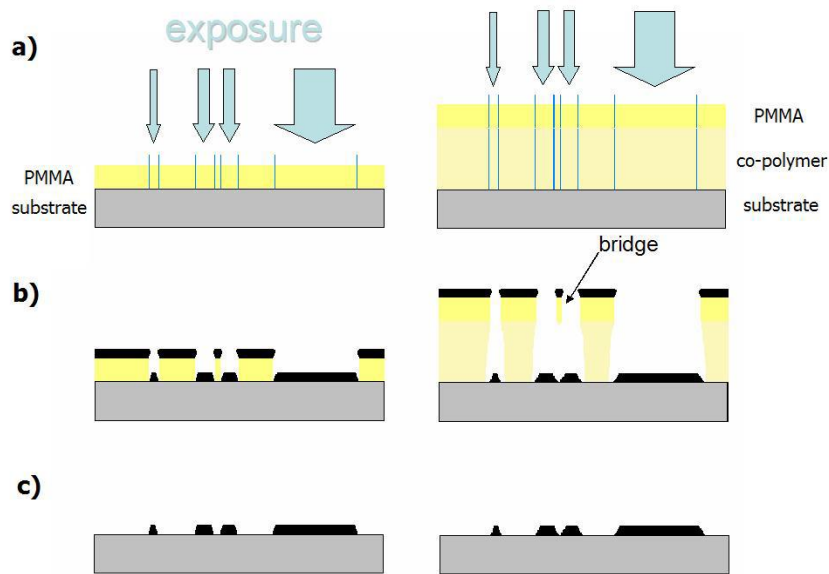Figure 4-1 illustrates the steps of the fabrication process for both single layer and double layer samples.

Figure 4-1: Electron-beam lithography and lift-off technology process steps.
(a) Exposure, (b) metal deposition and (c) lift-off.

The EBL was carried out on an AMRAY 1400 converted scanning electron microscope driven by the Nanometer Pattern Generator System by J. C. Nabity. Using a thermal emission tungsten cathode in the gun with 50 kV acceleration voltage, we have a lithography resolution of about 15-20 nm, a minimum line width of 30-35 nm and a minimum of 60-80 nm pitch. To develop the exposed image, we use a solution of methyl-isobuthyl ketone (MIBK), isopropanol (IPA) and methyl-ethyl ketone (MEK), 1:3:1.5% respectively, which has been identified as a high contrast developer by Bernstein et al. In Figure 4-1(b) the difference between the single layer and the double layer resist is shown by the larger undercut in the co-polymer. On the one hand, this can prevent the formation of thin, walls along the border of the dots as seen in Figure 4-2(a). On the other hand, the patterns are less defined in the presence of the co-polymer because of its larger shadow angle. As a result, the evaporated material that does not arrive perfectly perpendicular to the surface of the substrate most of the time, spreads out. Another property of the double layer resists is the development of PMMA bridges. These bridges appear to be quite elastic, and can cause pattern deformation if they stick together before evaporation as Figure 4-2(b) reveals. We evaporated cobalt or permalloy as

16

magnetic material in an Airco Temescal FC1800 e-beam evaporator. Both ferromagnetic materials have a melting point of around 1750 K. After evaporation, the lift-off is done in a mixture of methylene chloride (MC) and acetone (ACE) at a ratio of 8:1 respectively, at room temperature.
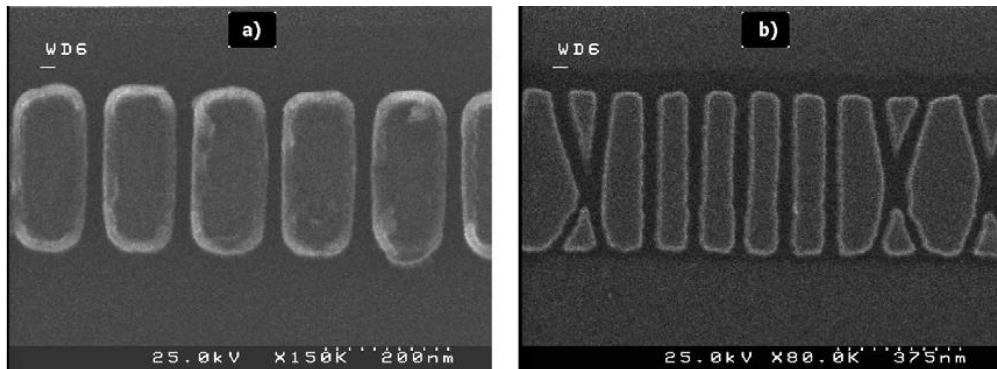

Figure 4-2: Top view SEM micrographs after lift-off. The elongated and flat, identically defined cobalt dots in the chains were fabricated (a) on single layer and (b) on double layer resist. In case of single-layer resist, there is material accumulation of the edges of the elements. In case of using double-layer resist, the pattern can get deformed as the PMMA bridges stick together.

Chapter 5

Results and Discussion

5.1   Maxwell Simulation Results

Below shown are the result of the simulation which has been performed in Ansys Maxwell 3D software. The environment chosen here is vacuum and all the simulations were done considering the vacuum only.
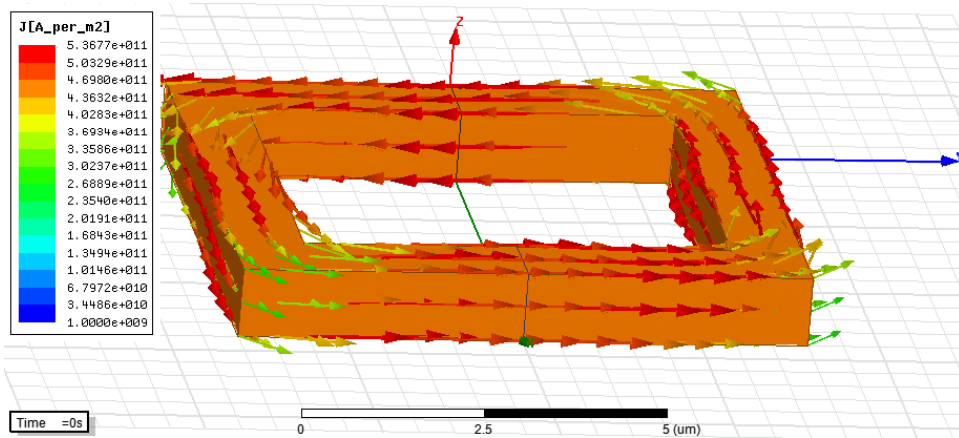

Figure 5-1: Maxwell 3D simulation result for the current density vector associated with the current flowing though the underlying conductor. The dimension of the wire chosen here is 1µm×1 µm

Given in Figure 5-1 is Maxwell simulation result simulated for the under lying conductor. The material here is chosen to be the copper wire the dimension of the cross section of which is taken as the 1µm×1 µm.

Figure 5-2 shows the 3D view of the field associated with the current flowing through the wire and the Figure 5-3 shows the side view of the field.
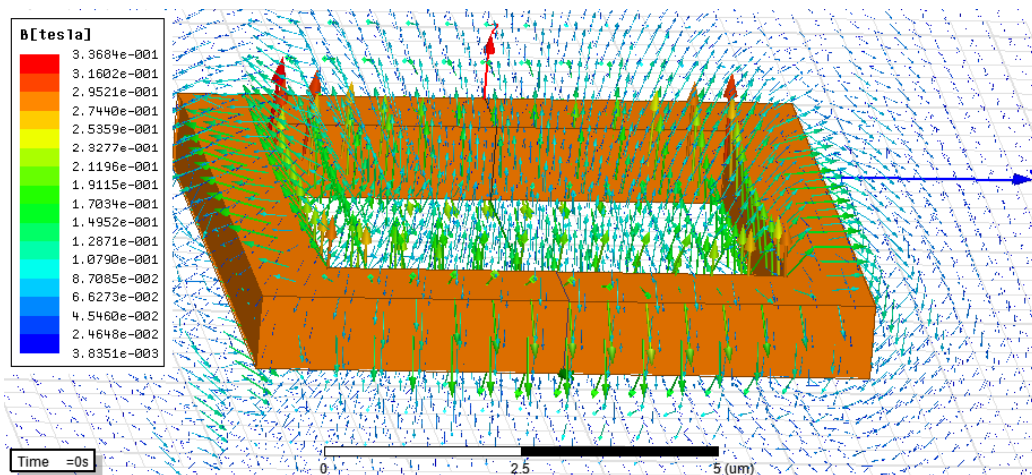
18

Figure 5-2: This is the 3D view of the field associated with the current flowing in the conductor. The maximum and the minimum value of the field associated with the given current density value are 336mT and 3.83mT respectively.
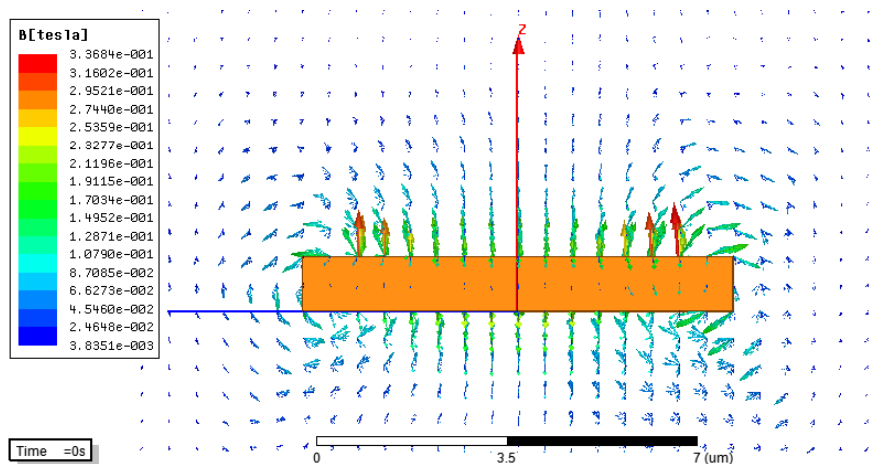

Figure 5-3: This is the 3D view of the field associated with the current flowing in the conductor. The maximum and the minimum value of the field associated with the given current density value are 336mT and 3.83mT respectively.

The current density as shown in the over is found to be maximum of 5.36×10^{11} A/m^2 and the field associated with is found to maximum of 336mT with placing any nanomagnetic dot over it.
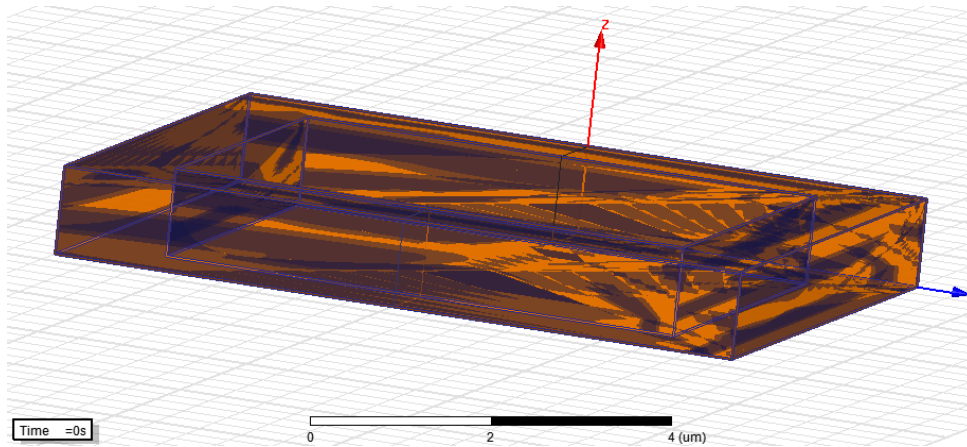
Figure 5-4: Insulation shown for the copper conductor over it before placing the nanomagnet dots so that there should be no electrical contact between dot and conductor.
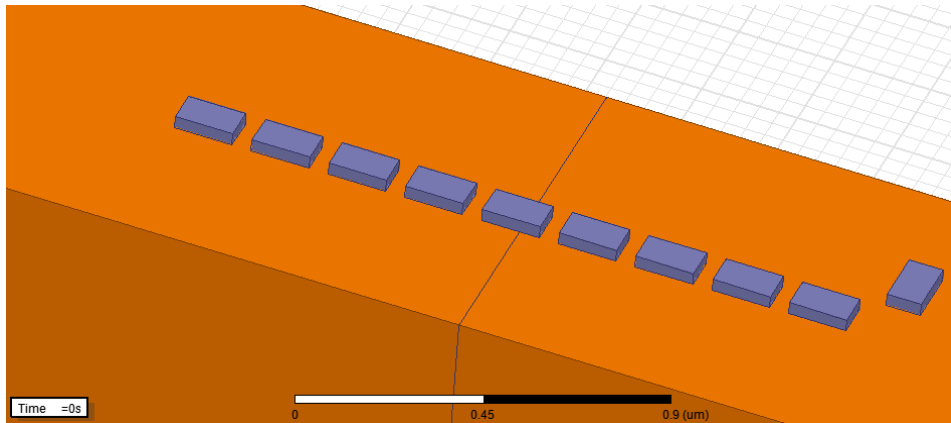

Figure 5-5: The Nanomagnetic dots are now placed over the copper conductor. The material chosen for the nanomagnetic dots was Fe with the relative permeability of 8000.

Figure 5-4 shows the insulation placed over the conductor before placing the nanomagnetic dots. Figure 5-5 shows the same copper conductor but with the nanomagnetic dots placed over it. The dimension of the nanomagnetic dots are chosen to be 110nm×50nm×30nm. Each of which were placed 20nm apart. They are placed in ferromagnetically coupled way. Figure 5-6 shows the simulated result for the same.
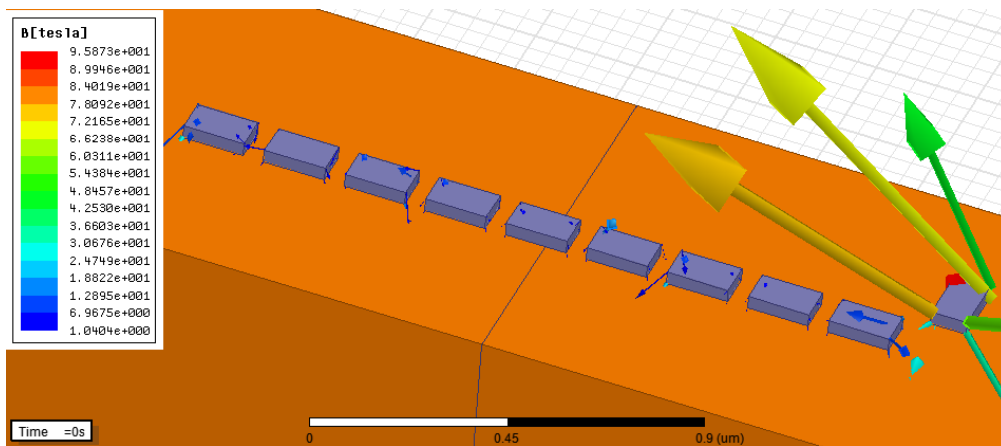
Figure 5-6: Simulation results shown with the Nanomagnetic dots placed over it. The simulation was ran for t = 1sec and the maximum and the minimum values of field associated with it are 95.87T and 1.04T respectively.

Below Table 5-1 shows the comparison result for the field associated in the conductor with and without the nanomagnetic dots placed over it.

Table 5-1: Comparison table for conductor with and without Nanomagnetic Dots placed over it for the same current density, J = 5.36×1011 A/m2

Field Value	Without Nanomagnetic Dots	With Nanomagnetic Dots
Maximum	336mT	95.87T
Minimum	3.83mT	1.04T

5.2   OOMMF Simulation Results

The simulations predict that the nanomagnets with various aspect ratios have different switching field values. Also the problems associated with the nanomagnet wires is that the signal propagation. As the simulation shown below the following are the problems associated with the propagation of the signals.
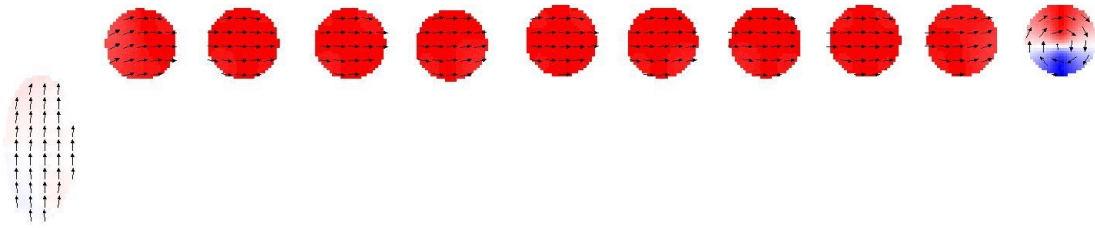
21

Figure 5-7: Driver magnet here is given 130mT in the positive y-direction of magnetic field is used to drive the circular nanomagnet wires and pass the signal but the signal does not passes after certain distance and it dies off.
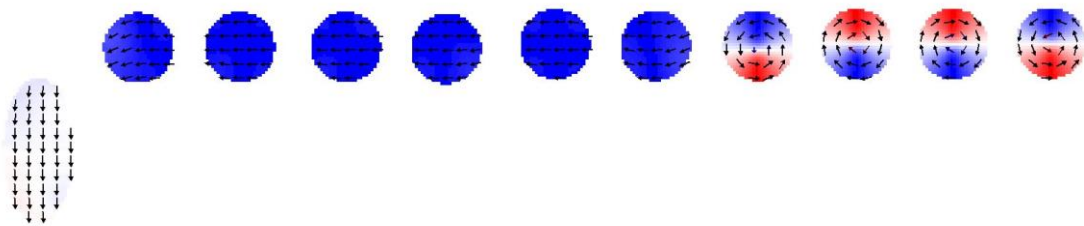

Figure 5-8: Same Driver magnet here is given 130mT in the negative y-direction of magnetic field is used to drive the circular nanomagnet wires and pass the signal but here also the signal does not passes after certain distance and it dies off.

As discussed in Chapter 3, the shape anisotropy can help for the above associated problem. The idea comes from the work of Varga et.al which is shown below. Given in Figure 5-9 is the structure of an unoptimized one-bit full adder built from 53 nanomagnets. Using shape anisotropy as discussed in Chapter 3, Varga et.al and his team has reduced the number of nanomagnets required to make the same adder as shown in Figure 5-10 the problems associated with the propagation of the signals.

The footprint can be reduced further by using asymmetric, slant magnets as inputs to the adder. The inputs are provided by the 7 slant magnets, and the number of the rounded edge magnets is only 14 (total of 21 magnets).
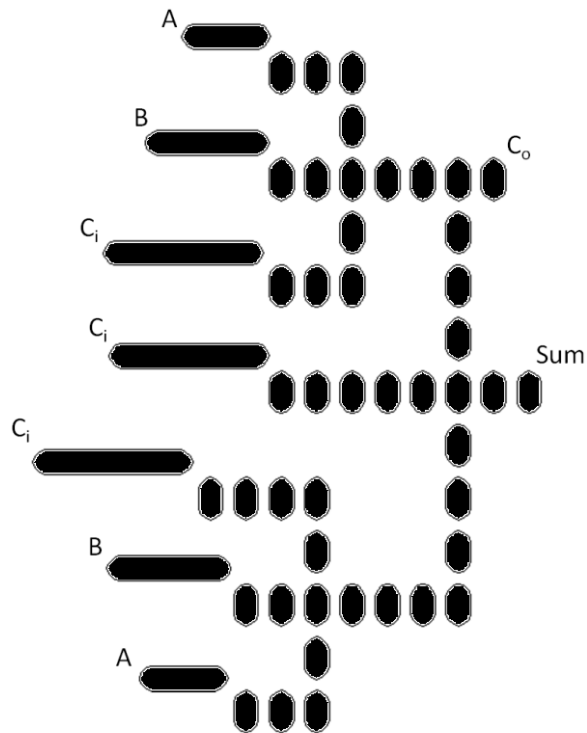
Figure 5-9: Schematic of the full adder including three, three-input majority gates, and several high aspect ratio magnets to act as drivers providing the input data (A, B, and Ci) for the circuit. The majority gates are the intersections of horizontal and vertical wires at which the center magnet is influenced by three input magnets (top, left and bottom neighbors) and influence an output magnet (right neighbor). The output is the sum (Sum) and the carry bit (Co).
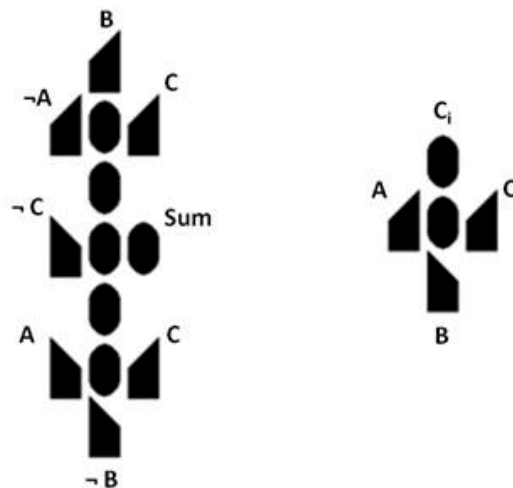

Figure 5-10: Reduced footprint design of the full adder. The inputs are provided by the slant magnets.

23

Using the idea as proposed by Varga .et.al and his team, this paper proposes the different ideas for the problems associated in the propagation of the signal by the nanomagnets, results of which has been discussed below.

The idea was to explore the phenomenal advantages of the shape anisotropy of the nanomagnet wires to solve the problems associated with the signal propagation. Using the shape anisotropy one can orient the easy axis in the direction he wishes. Shown in the Figure 5-11 is the one of the proposed methodology using the advantage of the shape anisotropy referring to what Varga .et.al has done in Figure 5-9 and Figure 5-10. Here, the driver magnet has the dimensions as 140nm×70nm×30nm. The dimensions of the wire shown is 1µm×70nm×30nm.

Figure 5-11: Driver magnet shown has the dimensions as 140nm×70nm×30nm. This driver is able to drive the wire of dimension 1µm×70nm×30nm.

The Domain Wall Conductor along with the standalone nanomagnets Figure 5-12 shows the fabricated structure of Domain Wall Conductor. Domain Wall Conductor are terminated with a pointed end to prevent the nucleation of a Domain Wall at this end. The Domain Wall injector is a 2.5µm diameter disk, which, when exposed to low magnitude magnetic fields, easily splits into multiple domains and can inject a wall into the Domain Wall Conductor. Referring to what Varga .et.al has done in Figure 5-12, this paper proposes another idea to possibly transmit the signal from one end to the other.

Figure 5-13 and Figure 5-14 shows the idea referring to what the Varga .et.al has done using Domain Wall Conductor in Figure 5-12.
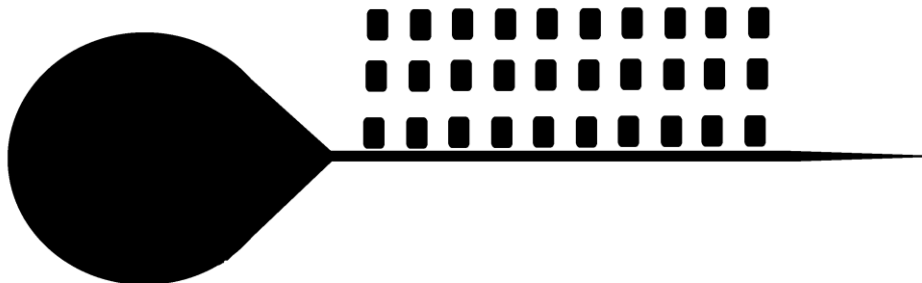

Figure 5-12: The domain wall conductor on the left has an expanded injector end

Figure 5-13: Removing the Domain wall and inserting the slant NanoMagnet Dot driver with injection
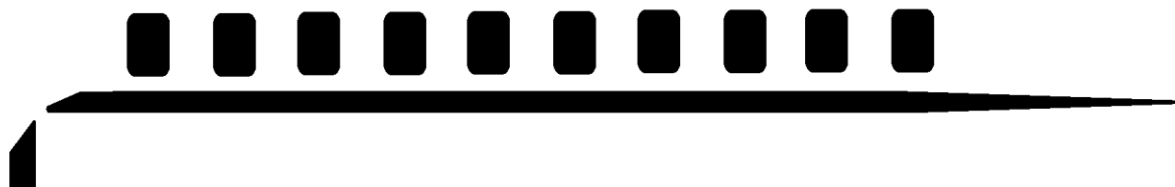
Figure 5-14: Along with the injection the and driver the NanoMagnet Dots to be driven are also added

Micro-magnetic simulations using NIST's OOMMF suite were performed to predict the behavior of the slant shaped wires and slant shaped drivers. Here are the results discussed below.

Here, the size of the driver magnet was given to be 140nm×70nm×30nm and the wire dimensions were 1µm×70nm×30nm. Figure 5-15 shows the simulation result for the driver magnet driving the

wire with the field strength of 130mT. The direction of the magnetic field in the driver in shown in the positive y-direction, thus the associated field in the wire is towards the right hand side. Similarly, Figure 5-16 shows the simulation result for the driver magnet driving the wire with the field strength of 130mT. The direction of the magnetic field in the driver here is in the negative y-direction, thus the associated field in the wire is towards the left hand side.
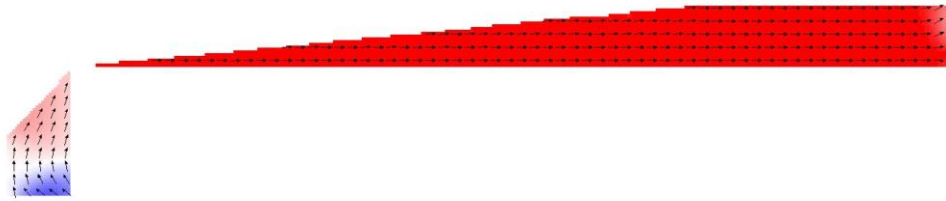
Figure 5-15: Driver driving the wire has the field strength of 130mT in the positive y-direction
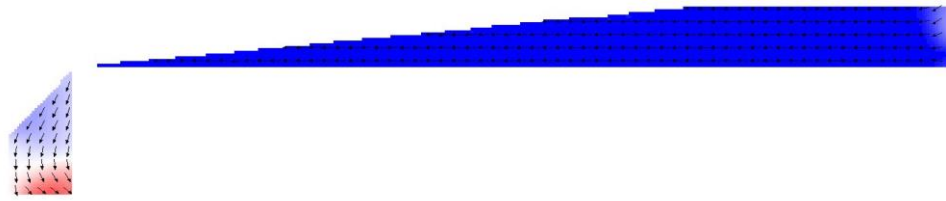
Figure 5-16: Driver driving the wire has the field strength of 130mT in the negative y-direction

For Figure 5-15 the simulation time came out to be 4.216ns and that for Figure 5-16 it came out to be 2.5462ns. Results have been compared in Table 5-2.

Table 5-2: Comparison Table

For	Positive y input	Negative y input
Demagnetization Energy	14240.6 J/m^3	14240.6 J/m^3
Exchange Energy	891.801 J/m^3	891.801 J/m^3
Simulation Time	4.216ns	2.5462ns

As discussed earlier about Domain Wall Conductor having diameter of 2.5µm and the injection of length of approximately 5µm as shown in Figure 5-12. Figure 5-17 and Figure 5-18 shows the simulation results when the applied in field is 100mT in either direction. Over this injection there are 30 nanomagnet dots each of which has the dimension 150nm×90nm×30nm.

Figure 5-17: Domain Wall Conductor driving the dots has the field strength of 100mT in the positive x-direction

Figure 5-18: Domain Wall Conductor driving the dots has the field strength of 100mT in the negative x-direction

Figure 5-19: Driver driving the injection has the field strength of 130mT in the positive x-direction with no Nanomagnet dots
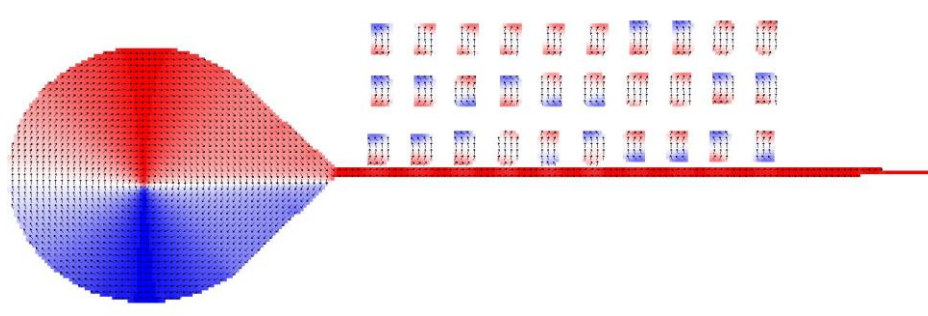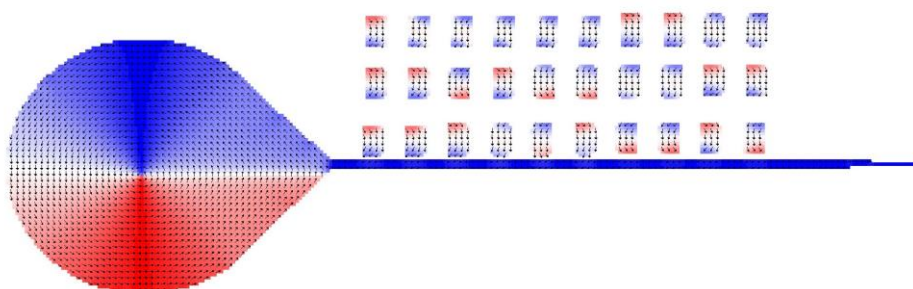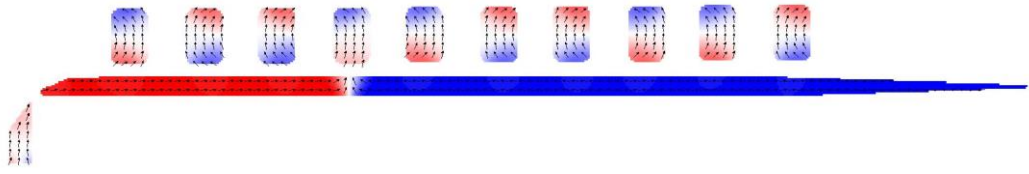
Figure 5-20: Driver driving the injection has the field strength of 500mT in the positive x-direction with 10 Nanomagnet Dots able to drive 4 Nanomagnet dots
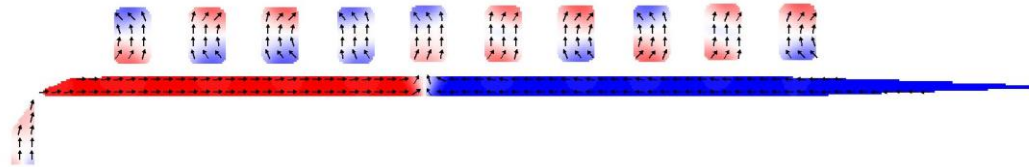
Figure 5-21: Driver driving the injection has the field strength of 650mT in the positive x-direction with 10 Nanomagnet Dots able to drive 5 Nanomagnet dots

Using their method, we have proposed an idea as shown in the Figure 5-13 and Figure 5-14 simulation results of which are are shown in the Figure 5-19, Figure 5-20 and Figure 5-21 and Table 5-3 and Table 5-4.

Table 5-3: Comparison Table for Existing and Proposed Idea

Parameter	Their Idea	Our Idea
Input Applied	100mT	650mT (Figure 5-21)
Simulation Time	13.533ns	6.9743ns

Table 5-4: Comparison Table for Our Proposed Idea

For Our Idea	Input Applied	Simulation Time	Dots Driven
Figure 5-19	130mT	5.788ns	NA
Figure 5-20	500mT	6.7243ns	4
Figure 5-21	650mT	6.9743ns	5

Chapter 6

Conclusion and Future work

This work introduces new methodologies to solve the issues related to propagation of the signal through Nanomagnet Logic Wires. The simulation using Maxwell 3D was done to verify the magnetic field associated with the current carrying conductor. The proposed idea is able to solve the problem associated with the propagation of the signal and has been verified using Micro Magnetic NIST's proposed OOMMF software and the results have been verified.

6.1 Future Scope

Future scope includes the problems associated with the speed. Still, the problem associated with the MQCA is the transition frequency cannot be beyond certain 100's of MHz, but the silicon transistors runs on GHz clock frequency.

Along with the frequency the current carrying conductor is also an issue because the resistance dominates when the cross section of metallic conductor is small. Also, the entire IC can be made out of the MQCA or not is still a question.

References

[1] C. Lent and P. Tougaw, "A device architecture for computing with quantum dots," Proc. of the IEEE, vol. 85, pp. 541 –557, apr 1997.

[2] A. O. Orlov, R. Kummamuru, R. Ramasubramaniam, C. S. Lent, G. H. Bernstein,and G. L. Snider, "Clocked quantum-dot cellular automata shift register," Surface Science, vol. 532-535, pp. 1193 – 1198, 2003. Proc. of the 7th Internl. Conf. on Nanometer-Scale Sc. and Tech. and the 21st European Conf. on Surface Science.

[3] M. Niemier and P. Kogge, "The 4-diamond circuit" - a minimally complex nanoscale computational building block in QCA," in VLSI, 2004. Proc. IEEE Computer society Annual Symp. on, pp. 3 – 10, feb 2004.

[4] V. Vankamamidi, M. Ottavi, and F. Lombardi, "A Line-Based Parallel Memory for QCA Implementation," IEEE Trans. On Nano., vol. 4, pp. 690–698, Nov. 2005.

[5] J. Timler and C. S. Lent, "Power gain and dissipation in quantum-dot cellular automata," Journ. of Appl. Phys., vol. 91, pp. 823–831, Jan 2002.

[6] P. D. Tougaw and C. S. Lent, "Dynamic behavior of quantum cellular automata," Journ. of Appl. Phys., vol. 80, pp. 4722–4736, oct 1996.

[7] S. Srivastava, S. Sarkar, and S. Bhanja, "Estimation of upper bound of power dissipation in qca circuits," Nano., IEEE Trans. on, vol. 8, no. 1, pp. 116 –127, 2009.

[8] "International technology roadmap for semiconductor," 2009.

[9] Q. Hang, Y. Wang, M. Lieberman, and G. H. Bernstein, "Molecular patterning through high-resolution polymethylmethacrylate masks," Applied Physics Letters, vol. 80, pp. 4220–+, Jun 2002.

[10] W. Hu, K. Sarveswaran, M. Lieberman, G. H. Bernstein, and S. Member, "High resolution electron beam lithography and dna nano-patterning for molecular qca," IEEE Trans. on Nano, vol. 4, pp. 312–316, 2005.

[11] C. S. Lent and B. Isaksen, "Clocked molecular quantum-dot cellular automata," Electron Dev., IEEE Trans. on, vol. 50, pp. 1890–1896, Aug. 2003.

[12] T. J. Dysart and P. M. Kogge, "Probabilistic analysis of a molecular quantum-dot cellular automata adder," Defect and Fault-Tolerance in VLSI Systems, IEEE Intl. Symp. on, vol. 0, pp. 478–486, 2007.

[13] C. S. Lent, P. D.Tougaw, W. Porod and G. H. Bernstein, "Quantum cellular automata," Nanotechnology 4, 49 (1993).

[14] V. Poulsen, "Magnetic Wire Recorder," patent # 661619, 1900.

[15] O. Smith, American engineer. He published one of the earliest works dealing with magnetic recording in 1888.

[16] W. J. Gallagher, S. S. P. Parkin, "Development of the magnetic tunnel junction MRAM at IBM: From first junctions to a 16-Mb MRAM demonstrator chip," IBM J. Res. Dev. 50, 5, 2006.

[17] S. S. P. Parkin, H. Masamitsu, T. Luc, "Magnetic domain-wall racetrack memory," Science, 320, 190-194, 2008.

[18] C. S. Lent, and P. D. Tougaw, "Device Architecture for Computing with Quantum Dots," Proc. IEEE 85, 541, 1997.

[19] R. J. Spain, "Controlled Domain Tip Propagation," part I., J. Appl. Phys. 37, 2572, 1966.

[20] R. J. Spain and H. I. Jauvtis, "Controlled Domain Tip Propagation," part II, J. Appl. Phys. 37, 2584, 1966.

[21] G. Csaba, W. Porod, and A.I. Csurgay, "A Computing Architecture Composed of Field-Coupled Single Domain Nanomagnets Clocked by Magnetic Field," Int. J. Circ. Theor. Appl. 31, 67–82, 2003.

[22] A. Dingler, M. J. Siddiq, M. T. Niemier, X. S. Hu, M. T. Alam, G. H. Bernstein, and W. Porod, "Controlling Magnetic Circuits: How Clock Structure Implementation Will Impact Logical Correctness and Power", IEEE Symp. on Nanoarch. 21-26, 2009.

[23] C. S. Lent, P. D. Tougaw, W. Porod and G. H. Bernstein, "Quantum Cellular Automata," Nanotechnology 4, 49, 1993.

[24] R. P. Cowburn, and M. E. Welland, "Room Temperature Magnetic Quantum Cellular Automata," Science 287, 1466, 2000.

[25] D. A. Allwood, G. Xiong, M. D. Cooke, C. C. Faulkner, D. Atkinson, N. Vernier, R. and P. Cowburn, "Submicrometer Ferromagnetic NOT Gate and Shift Register," Science 296, 2002.

[26] A. Imre, G. Csaba, L. Ji, A. Orlov, G. H. Bernstein, and W. Porod, "Majority Logic Gate for Magnetic Quantum-Dot Cellular Automata," Science, 310, 205-208, 2006.

[27] M. T. Niemier, X. S. Hu, and M. T. Alam, "Clocking Structures and Power Analysis for Nanomagnet-Based Logic Devices," Proc. of the 2007 International Symposium on low power electronics and design 26-31, 2007.

[28] M. T. Alam, M. J. Siddiq, G. H. Bernstein, M. Niemier, W. Porod, and X. S. Hu, "On-chip clocking for nanomagnet logic devices, " IEEE Transactions on Nanotechnology, 9, 3, 348-351, 2010.

[29] H. Koop, H. Brückl, D. Meyners, and G. Reiss, "Shape Dependence of Magnetization Reversal in Sub-μm Magnetic Tunnel Junctions," J. of Magn. and Magn. Mat. 272-276, 2004.

[30] A. Imre, "Experimental Study of Nanomagnets for Magnetic Quantum-Dot Cellular Automata (MQCA) Logic Applications," Ph.D. thesis, University of Notre Dame, IN, 2005.

[31] G. Csaba, M. Becherer, W. Porod, "Development of CAD Tools for Nanomagnetic Logic Devices", accepted for International Journal of Circuit Theory and Applications, 2011.

[32] A. Orlov, A. Imre, G. Csaba, L. Ji, W. Porod, and G. H. Bernstein, "Magnetic Quantum-Dot Cellular Automata: Recent Developments and Prospects," Journal of Nanoelectronics and Optoelectronics, vol. 3, no. 1, pp. 55–68, 2008.

[33] C. T. Rettner, S. Anders, T. Thomson, M. Albrecht, Y. Ikeda, M. E. Best, and B. D. Terris, "Magnetic characterization and recording properties of patterned Co70Cr18Pt12 perpendicular media," IEEE Trans. Mag. 38, 1725 (2002).

[34] G. Xiong, D. A. Allwood, M. D. Cooke, and R. P. Cowburn, "Magnetic nanoelements for magnetoelectronics made by focused-ion beam milling," Appl. Phys. Lett. 79, 3461 (2001)

[35] C. A. Ross, M. Hwang, M. Shima, J. Y. Cheng, M. Farhoud, T. A. Savas, H. I. Smith, W. Schwarzacher, F. M. Ross, M. Redjdal, and F. B. Humphrey, "Micromagnetic behavior of electrodeposited cylinder arrays," Phys. Rev. B. 65, 144417 (2002)

[36] O. Donzelli, D. Palmeri, L. Musa, F. Casoli, F. Albertini, L. Pareti, and G. Turilli, "Perpendicular magnetic anisotropy and stripe domains in ultrathin Co/Au sputtered multilayers," Journ. Appl. Phys. 93, 9908 (2003)

[37] J. R. Barnes, S. J. O'Shea, M. E. Welland, J. Y. Kim, J. E. Evetts, and R. E. Somekh, "Magnetic force microscopy of Co-Pd multilayers with perpendicular anisotropy," Journ. Appl. Phys. 76, 2974 (1994)

[38] T. Aoyama, K. Uchiyama, T. Kagotani, K. Hattori, Y. Wada, S. Okawa, H. Hatate, H. Nishio, I. Sato, "Fabrication and properties of CoPt patterned media with perpendicular magnetic anisotropy," IEEE Trans. Mag. 37, 1646 (2001)